



भारतीय
प्रौद्योगिकी
संस्थान
काशी हिन्दू विश्वविद्यालय



INDIAN
INSTITUTE OF
TECHNOLOGY
BANARAS HINDU UNIVERSITY

CERTIFICATE

It is certified that the work contained in the thesis titled "*Study of Magnetic and Transport Properties of Some Topological materials*" by *Mahima Singh* has been carried out under my supervision and that this work has not been submitted elsewhere for a degree.

It is further certified that the student has fulfilled all the requirements of comprehensive examination, candidacy and SOTA for the award of Ph.D. Degree.

Signature:


31.12.21

Supervisor

Sandip Chatterjee

(Professor)

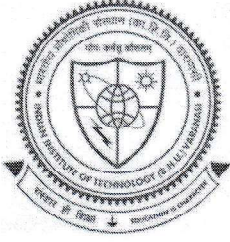
Department of Physics

Indian Institute of Technology

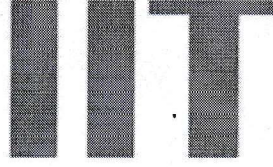
(Banaras Hindu University)

Varanasi-221005 (UP)

Professor
Department of Physics
Indian Institute of Technology
(Banaras Hindu University)
Varanasi-221005



भारतीय
प्रौद्योगिकी
संस्थान
काशी हिन्दू विश्वविद्यालय



INDIAN
INSTITUTE OF
TECHNOLOGY
BANARAS HINDU UNIVERSITY

DECLARATION BY THE CANDIDATE

I, "**Mahima Singh**", certify that the work embodied in this thesis is my own bonafide work and carried out by me under the supervision of "**Prof. Sandip Chatterjee**" from "**July 2016**" to "**December 2021**", at the "**Department of Physics**", Indian Institute of Technology (BHU), Varanasi. The matter embodied in this thesis has not been submitted for the award of any other degree/diploma. I declare that I have faithfully acknowledged and given credits to the research workers wherever their works have been cited in my work in this thesis. I further declare that I have not willfully copied any other's work, paragraphs, text, data, results, *etc.*, reported in journals, books, magazines, reports dissertations, theses, *etc.*, or available at websites and have not included them in this thesis and have not cited as my own work.

Date: 31-12-2021

Place: IIT (BHU), Varanasi

Signature of the student

(Mahima Singh)

CERTIFICATE BY THE SUPERVISOR

It is certified that the above statement made by the student is correct to the best of my/our knowledge.

Supervisor

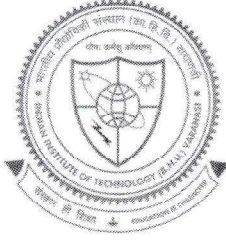
Sandip Chatterjee

(Professor)

Department of Physics
Indian Institute of Technology
(Banaras Hindu University)
Varanasi-221005

Signature of Head of Department

HEAD/विभागाध्यक्ष
भौतिकी विभाग/Deptt. of Physics
मा.प्रौ.सं./का.हि.वि./IIT (BHU)
वाराणसी/Varanasi-221005



COPYRIGHT TRANSFER CERTIFICATE

Title of the Thesis: *Study of Magnetic and Transport Properties of Some Topological materials*

Name of the Student: *Mahima Singh*

Copyright Transfer

The undersigned hereby assigns to the Indian Institute of Technology (Banaras Hindu University) Varanasi all rights under copyright that may exist in and for the above thesis submitted for the award of the “*DOCTOR OF PHILOSOPHY*”.



Date: 31-12-2021

Place: IIT (BHU), Varanasi

Signature of the Student

(*Mahima Singh*)

Note: However, the author may reproduce or authorize others to reproduce material extracted verbatim from the thesis or derivative of the thesis for the author's personal use provided that the source and the Institute's copyright notice are indicated.

Acknowledgements

The journey of PhD has been a turning point of my life, and it would not be possible without the constant support, assistance and guidance that I have received from countless people. I would like to take this opportunity to acknowledge and appreciate those people who have given their valuable time during my PhD.

I am indebted to my thesis supervisor Prof. Sandip Chatterjee for his constant monitoring, enthusiastic encouragement, continued guidance, and unconditional support throughout my PhD journey. His ingenious approach to research is a source of inspiration, and this approach is reflected in his simple but clear writing style, which I want to carry forward in my career. His calmness, enormous knowledge and patience over the last five years will always remain as a happy memory.

I am thankful to my RPEC members, Dr. B. N. Pal and Dr. S. Patil, for their knowledgeable, motivational and umpteen suggestions throughout this research work.

I want to express my gratitude towards the Head of Department for providing me required facilities of the department. I also wish to thank all the faculty members of the Department of Physics, IIT (BHU) Varanasi for their motivation, selfless support and suggestions during my Ph.D. time.

I would also like to thank CIFIC, IIT (BHU) for providing experimental facilities during the entire course of research work.

I am also grateful to Dr. Shiv Kumar and Dr. P. Shahi for furnishing extraordinary measurement facilities abroad to execute the thesis work. Without their support, it could have been impossible to complete this thesis adequately.

Acknowledgements

Furthermore, I would also like to express my extreme gratefulness towards my senior research member Dr. R. Singh, Dr. A. Singh, Dr. A. Pal, Dr. Vinod Gangwar, Dr. Prajyoti Singh and other lab members, Mohd. Alam, Mrs. L. Ghosh, Ms. Seema, Ms. D. Pal, Mr. S. Vijay, Ms. Srishti, Mr. Dheeraj, Mr. Rahul, Ms. Neha, Ms. Swangsiddha Ghosh, and Mr. Sambhab for sharing their knowledge and creating a pleasant lab environment. I would also like to thank all research colleagues of the Department of Physics, IIT (BHU), and Special thanks to my friends Vandna Tomar, Khayati Mourya, Divya Prakash Dubey, Mohit Goel, Puja Saxena, Akanksha Yadav, Khyati Anand, Yamini K. Rao, Dipti Gangwar, for their awesome and pleasant company and confidence to complete this work with laughter. My Parents (Shri Krishna Pal Singh, Smt. Geeta Gangwar and Smt. Sonam Garg) and siblings (Ayu, Sona, Kannu and Shivi), who are the strong pillars of my life, are always there with me during the Whole journey. I also want to extend my gratitude towards my husband, Himanshu Garg whose continuous support, love and motivation gave me the strength to complete my work on time.

I am also thankful to all the technical, non-teaching as well as office staff of the Department of Physics, IIT (BHU) Varanasi for their assistance when required.

I would also like to acknowledge the funding agency Indian Institute of Technology BHU for the teaching assistantship.

Finally, I am grateful to Almighty for giving me the patience to make this endeavor a success.

(Mahima Singh)

*I dedicate this thesis to my Brother (Kanishk) and mother (Geeta) for
their selfless love.*

Contents

Certificate	ii
Declaration by the Candidate	iii
Copyright Transfer Certificate	iv
Acknowledgements	v
Contents	ix
List of Figures	xii
List of Tables	xviii
Preface	xix
Chapter 1: Introduction: A bibliographic review	23-51
1.1 Introduction	23
1.2 Topology	25
1.3. Berry Phase and Chern number	27
1.4 Time Reversal Symmetry (TRS)	27
1.5 Background of Topological Insulator	28
1.5.1 Hall Effect	28
1.5.2 Effect of the magnetic field in 3D system	30
1.5.3 Effect of the magnetic field in 2D system	32
1.5.4 Quantum Hall Effects (QHE)	32
1.5.5 Quantum Spin Hall Effect (QSHE)	34
1.5.6 Spin-orbit coupling	37
1.5.7 Quantum Anomalous Hall Effect (QAHE)	38
1.5.8 Shubnikov-de Haas (SdH) Oscillations	40
1.5.9 Weak Localization (WL) and Weak Antilocalization (WAL) Effects	41
1.6 Historical Developments of 2D and 3D Topological Insulators	42
1.6.1 The first 2D topological insulator HgTe	42
1.6.2 3D Topological Insulators	44
1.6.3 The First 3D Topological Insulator $\text{Bi}_{1-x}\text{Sb}_x$	44
1.6.4 New materials Bi_2Se_3 , Bi_2Te_3 and Sb_2Te_3	46
1.6.5 Crystal structure and Symmetry Properties	47
Chapter 2: Sample Synthesis and Characterization Tools	53-66
2.1 Introduction	54
2.2 Sample synthesis of TIs	54
2.3 Experimental characterization tools	55
2.3.1 X-Ray diffraction (XRD)	55
2.3.2 Laue diffraction pattern	57

Contents

2.3.3 Transport properties measurements	58
2.3.3.1 Electric resistivity (ρ_{xx})	58
2.3.3.2 Hall resistivity (ρ_{xy})	59
2.3.3.3 Thermoelectric measurement	60
2.3.4 Magnetic property measurement System (MPMS)	61
2.3.5 Photoemission Spectroscopy	63
2.3.5.1 Angle-resolved photoemission spectroscopy (ARPES)	65
Chapter 3: Evidence of surface and bulk magnetic ordering in Fe and Mn doped $\text{Bi}_2(\text{SeS})_3$ topological insulator	67-83
3.1 Introduction	69
3.2 Experimental details	70
3.3 Results and discussions	72
3.3.1 Experimental Study	72
3.3.2 Theoretical Study	81
3.4 Conclusion	82
Chapter 4: Anomalous Hall effect in Cu doped Bi_2Te_3 Topological Insulator	84-107
4.1 Introduction	86
4.2 Experimental details	87
4.3 Results and Discussion	88
4.4 Conclusion	107
Chapter 5: Correlation between change-over from Weak Anti Localization (WAL) to Weak Localization (WL) and coexistence of positive and negative magneto-resistance in S-doped $\text{Bi}_{1.5}\text{Sb}_{0.5}\text{Te}_{1.3}\text{Se}_{1.7}$	108-125
5.1 Introduction	110
5.2 Experimental	111
5.3 Results and Discussion	112
5.4 Conclusion	124
Chapter 6: The study of Raman and transport properties in Fe doped $\text{Bi}_2(\text{SeS})_3$	126-144
6.1 Introduction	128
6.2 Experimental details	129
6.3 Results and Discussion	129
6.3.1 Raman study	140
6.4 Conclusion	143

Contents

Chapter 7: Summary and future perspectives	145-149
8.1 Summary	147
8.2 Future perspectives	148
References	150-164
List of Publications	165
Schools / Meetings / Workshops / Conference Attended	166

List of Figures

- Figure 1.1:** Band diagram for metal, semiconductor and insulator 23
- Figure 1.2:** Schematic representation of topology showing smooth deformation from cup to doughnut. 25
- Figure 1.3:** The sphere and the doughnut are topologically non-equivalent and have different genus numbers. 26
- Figure 1.4:** schematic diagram of motion of two electrons having opposite spins with preservation of TRS in TSS. 28
- Figure 1.5:** Schematic diagram of Hall effect. 30
- Figure 1.6:** Energy band diagram for electrons vs. wave vector for different Landau levels in 3D system. 31
- Figure 1.7:** Quantization of energy levels into discrete Landau levels under the applied magnetic field (left) and the variation in longitudinal (ρ_{xx}) and transverse resistivity (ρ_{xy}) with applied magnetic field showing QHE. 33
- Figure 1.8:** Skipping orbits at the edge state and cyclotron orbits in bulk in 2D electron gas in the presence of the magnetic field. 34
- Figure 1.9:** Two copies of the quantum Hall effect (QHE) with the opposite magnetic field (left) and (right) the amalgamation of these two QHE states makes a quantum spin Hall effect (QSHE) without applied magnetic field 35
- Figure 1.10:** (Left) QHE with both right moving and left moving edge states. These states are robust against backscattering. (Right) QSHE with upper state right moving spin up and left moving spin down. Backscattering is suppressed from nonmagnetic impurities. 35
- Figure 1.11:** schematic diagram of two opposite scattering paths around an impurity for the QSH state. The total path difference between them is 2π , leading to suppression of the backscattering for Fermions. 36
- Figure 1.12:** schematic diagram of insulating state with a bandgap between the conduction and valence band (b) bulk is insulating but skipping orbits at the edges allows the conduction of electron giving rise to the conduction i.e. no band gap (c) in QSHE, both type of left and right moving path having opposite spins are allowed which is protected by time-reversal symmetry. 37
- Figure 1.13:** The variation of Hall resistivity ρ_{xy} with the applied magnetic field B . (a) ordinary Hall effect (b) anomalous Hall effect (AHE) (c) measured hysteresis loop from quantum anomalous Hall effect (QAHE). 39
- Figure 1.14:** (a) The two time-reversed scattering loops without spin-momentum locking exhibiting weak localization in magnetoconductivity ($\Delta G(B)$). (b) The two time-

List of Figures

reversed scattering loops with spin-momentum locking exhibited weak antilocalization in ΔG (B). 42

Figure 1.15: (a) bulk energy bands for HgTe and CdTe at Γ point (b) CdTe/HgTe/CdTe quantum well in normal regime $d < d_c$ and in inverted regime $d > d_c$. 43

Figure 1.16: The surface band dispersion second-derivative image of $\text{Bi}_{0.9}\text{Sb}_{0.1}$. There are five crossing between Γ and M which confirms topological non-trivial surface state. 46

Figure 1.17: Calculated band structure of Sb_2Se_3 , Sb_2Te_3 , Bi_2Se_3 and Bi_2Te_3 by *ab initio* density functional theory. Red represents occupied bulk and surface states, and blue signifies bulk band gap. 47

Figure 1.18: (a) Crystal structure of Bi_2Se_3 , the red box shows single quintuple layer (b) shows that three different A, B, and C sites are assigned to a triangular lattice in one quintuple layer (c) Se and Bi atoms are arranged in a sequence in quintuple layer. 49

Figure 1.19: Schematic picture of the band inversion of Bi and Se p orbitals in Bi_2Se_3 at the Γ point. Stage I represents the effect of chemical bonding, Stage II represents the crystal field splitting, Stage III represents the effect of SOC. 50

Figure 2.1: (a) Flow chart of synthesis process (b) Photograph of cleaved crystal sample. 55

Figure 2.2: (a) Photographic demonstration of Bragg's law (b) Actual photograph of Rigaku Mini Flex II DESKTOP X-ray diffractometer set up. 56

Figure 2.3: Schematic diagram of (a) Transmission Laue diffraction geometry (b) Back-reflection Laue diffraction geometry. 57

Figure 2.4: Schematic of four-probe measurement geometry. 58

Figure 2.5: Schematic diagram for Hall Effect measurement. 60

Figure 2.6: Schematic diagram of sample holder for thermoelectric measurement. Temperature difference at the both ends of the sample creates a temperature gradient. 61

Figure 2.7: (a) Schematic diagram of SQUID-VSM detection system (b) Photograph of actual QD-MPMS measurement system. 63

Figure 2.8: Illustrational of photoemission process. 64

Figure 2.9: (a) Schematic of ARPES measurement setup (b) Shows ARPES spectra of pure Bi_2Se_3 TI. 66

List of Figures

- Figure 3.1:** XRD pattern for all the prepared single crystal samples cleaved along (00l) plane. 71
- Figure 3.2:** The variation of Hall resistivity as a function of applied magnetic field a) $x=0.06$, (b) $x=0.18$ for $\text{Bi}_{2-x}\text{Fe}_x\text{Se}_{2.79}\text{S}_{0.21}$, (c) 0.18 for $\text{Bi}_{2-x}\text{Mn}_x\text{Se}_{2.79}\text{S}_{0.21}$ at different temperatures. 73
- Figure 3.3:** ARPES spectra for (a) $x=0.06$, (b) $x=0.12$, (c) $x=0.18$, and (d) 0.24 of $\text{Bi}_{2-x}\text{Fe}_x\text{Se}_{2.79}\text{S}_{0.21}$. 74
- Figure 3.4:** ARPES spectra for (a), (b) for $x=0.12$, (c), (d) for $x=0.18$ of $\text{Bi}_{2-x}\text{Mn}_x\text{Se}_{2.79}\text{S}_{0.21}$. 76
- Figure 3.5:** Magnetization (M) as a function of applied magnetic field (H) of $\text{Bi}_{2-x}\text{Fe}_x\text{Se}_{2.79}\text{S}_{0.21}$ with (a) $x=0.06$, (b) $x=0.12$, (c) $x=0.18$, (d) 0.24 and of $\text{Bi}_{2-x}\text{Mn}_x\text{Se}_{2.79}\text{S}_{0.21}$ for (e) $x=0.12$, (f) $x=0.18$ at different temperatures. 78
- Figure 3.6:** (a) magnetization vs. temperature (M-T (ZFC)) curve of $\text{Bi}_{2-x}\text{Fe}_x\text{Se}_{2.79}\text{S}_{0.21}$. The Variation of Magnetic Susceptibility as a function of temperature (b) $\text{Bi}_{1.88}\text{Mn}_{0.12}\text{Se}_{2.79}\text{S}_{0.21}$ (c) $\text{Bi}_{1.82}\text{Mn}_{0.18}\text{Se}_{2.79}\text{S}_{0.21}$ (d) MFM image of $\text{Bi}_{2-x}\text{Fe}_x\text{Se}_{2.79}\text{S}_{0.21}$, for $x=0.06$ and (e) for $x=0.18$ (f) Arrott plot of $\text{Bi}_{2-x}\text{Fe}_x\text{Se}_{2.79}\text{S}_{0.21}$, for $x=0.06$ and (g) $x=0.18$. 79
- Figure 3.7:** Density of States (DOS) from DFT Calculation for (a) $\text{Bi}_{1.82}\text{Fe}_{0.18}\text{Se}_{2.79}\text{S}_{0.21}$ and (b) $\text{Bi}_{1.82}\text{Mn}_{0.18}\text{Se}_{2.79}\text{S}_{0.21}$. 82
- Figure 4.1:** X-ray diffraction pattern of $\text{Bi}_2\text{Cu}_x\text{Te}_{3-x}$ topological insulators and Laue diffraction Pattern. 88
- Figure 4.2:** ARPES spectra for $x = 0.03$ (a) and 0.15 (b) of $\text{Bi}_2\text{Cu}_x\text{Te}_{3-x}$. (c) and (d) Show the electron distribution curve. 90
- Figure 4.3:** Constant energy contours of $\text{Bi}_2\text{Cu}_x\text{Te}_{3-x}$ at the Fermi energy for (a) $x = 0.03$ and (b) 0.15 from ARPES measurement. (c) and (d) Show the stacked plots of the constant energy contours at different binding energies. 92
- Figure 4.4:** Temperature variation of resistivity of $\text{Bi}_2\text{Cu}_x\text{Te}_{3-x}$ for (a) $x = 0.03$ and (b) 0.09 . 94
- Figure 4.5:** Magnetic field variation of magnetoresistance of $\text{Bi}_2\text{Cu}_x\text{Te}_{3-x}$ for (a) $x = 0.03$ and (b) 0.09 at different temperatures. 96
- Figure 4.6:** (a) SdH oscillations (b) Landau level fan diagram (c) first Fourier transform curve (d) L-K fitting curve and average calculated cyclotron mass (m_{cyc}) [in inset of (d)] of $\text{Bi}_2\text{Cu}_x\text{Te}_{3-x}$ for $x = 0.03$. 97

List of Figures

Figure 4.7: (a) SdH oscillations (b) Landau level fan diagram (c) first Fourier transform curve (d) L–K fitting curve and cyclotron mass calculation [in inset of (d)] of $\text{Bi}_2\text{Cu}_x\text{Te}_{3-x}$ for $x = 0.09$. 98

Figure 4.8: The variation of Hall resistivity as a function of applied magnetic fields of $\text{Bi}_2\text{Cu}_x\text{Te}_{3-x}$ for (a) $x = 0$, (b) $x = 0.03$ (c) $x = 0.09$ and (d) $x = 0.15$ at different temperatures. 102

Figure 4.9: Calculated anomalous Hall effect (AHE) of $\text{Bi}_2\text{Cu}_x\text{Te}_3$ for (a) $x = 0.03$ and (b) 0.09 at different temperatures. (c) and (d) Estimated AHE at diff. temperatures of $\text{Bi}_2\text{Cu}_x\text{Te}_{3-x}$ for $x = 0.03, 0.09, 0.15$ at 10 K and 100 K. 103

Figure 4.10: (a) Magnetization vs. temperature ($M - T$) and (b) magnetization (M) vs applied magnetic field ($M - H$) of $\text{Bi}_2\text{Cu}_x\text{Te}_{3-x}$ (with $x = 0.03, 0.09$ and 0.15). 105

Figure 4.11: (a) and (c) The variation between σ_{xx} and σ_{AHE} and (b), (d) temperature variation of tangent of anomalous Hall angle [$\tan(\theta_{\text{AHE}})$] for $\text{Bi}_2\text{Cu}_x\text{Te}_{3-x}$ respectively for $x = 0.03$ and 0.09 . 106

Figure 5.1: (a) X-ray diffraction pattern of $\text{Bi}_{1.5}\text{Sb}_{0.5}\text{Te}_{1.3}\text{Se}_{1.7-y}\text{S}_y$ Topological insulators (b) Laue pattern of BSTSS-5 and (c) BSTSS-10. 113

Figure 5.2: (a) and (b) Resistivity variation with temperature of BSTSS-5 and BSTSS-10. 114

Figure 5.3: (a) and (c) Arrhenius Fitting of BSTS-5 and BSTS-10 (b) and (d) VRH fitting BSTS-5 and BSTS-10. 115

Figure 5.4: The variation of Hall resistivity as a function of applied magnetic fields of $\text{Bi}_{1.5}\text{Sb}_{0.5}\text{Te}_{1.3}\text{Se}_{1.7-y}\text{S}_y$ (a) BSTSS-5, (b) BSTSS-10 at different temperatures (mobility vs. Temperature curve in inset). 116

Figure 5.5: Magnetic Fig. field Variation of Magnetoresistance of $\text{Bi}_{1.5}\text{Sb}_{0.5}\text{Te}_{1.3}\text{Se}_{1.7-y}\text{S}_y$ (a) BSTSS-5 and (b) BSTSS-10 at different temperatures; WAL fitting (c) and (d) for BSTSS-5 and (e) and (f) BSTSS-10 at different temperatures; Fitting for n-MR correction (g) BSTSS-5 and (h) BSTSS-10. 119

Figure 5.6: (a) and (b) ARPES spectra for BSTSS-5 and BSTSS-10 (c) and (d) Lorentzian Fit for BSTSS-5 and BSTSS-10 respectively. 124

Figure 6.1: Temperature Variation of resistivity of $\text{Bi}_{2-x}\text{Fe}_x\text{Se}_{3-y}\text{S}_y$ for (a) $x=0.06$, (b) $x=0.12$, (c) $x=0.18$, and (d) 0.24 . 131

Figure 6.2: Magnetic field Variation of Magnetoresistance of $\text{Bi}_{2-x}\text{Fe}_x\text{Se}_{3-y}\text{S}_y$ for (a) $x=0.06$, (b) $x=0.12$, (c) $x=0.18$, and (d) 0.24 at different temperatures. 132

Figure 6.3: Magnetic field Variation of Magnetoresistance of $\text{Bi}_{2-x}\text{Mn}_x\text{Se}_{3-y}\text{S}_y$ for (a) $x=0.12$, (b) $x=0.18$ at different temperatures. 133

List of Figures

Figure 6.4: Landau Level Fan diagram of $\text{Bi}_{2-x}\text{Fe}_x\text{Se}_{3-y}\text{S}_y$ (a) $x=0.06$, (b) $x=0.12$, (c) $x=0.18$, and (d) 0.24 . 136

Figure 6.5: Kohler scaling of $\text{Bi}_{2-x}\text{Fe}_x\text{Se}_{3-y}\text{S}_y$. (a) $x=0.06$, (b) $x=0.12$, (c) $x=0.18$, and (d) 0.24 . 137

Figure 6.6: (a) Measured value of Seebeck coefficient for all the samples and calculated value of power factor with respect to temperature (b) $x=0.06$, (c) $x=0.12$, (d) $x=0.18$, and (e) 0.24 . 139

Figure 6.7: Temperature dependent Raman Spectra for (a) $x=0.06$, (b) $x=0.18$. 141

Figure 6.8: Variation of Peak positions and FWHM with the Raman shift (a) $x=0.06$, (b) $x=0.18$. 142

List of Tables

- Table-3.1:** The obtained different parameters from ARPES and Hall effect measurements. 75
- Table 4.1:** Lattice parameters of $\text{Bi}_2\text{Cu}_x\text{Te}_{3-x}$ (with $x = 0, 0.03, 0.09$ and 0.15) obtained from the Reitveld refinement. 88
- Table 4.2:** Obtained parameters of $\text{Bi}_2\text{Cu}_x\text{Te}_{3-x}$ (with $x = 0.03$ and 0.09) from SdH oscillations, first Fourier transform calculation and Hall effect measurements. 99
- Table 4.3:** Different parameters of $\text{Bi}_2\text{Cu}_x\text{Te}_{3-x}$ (with $x = 0, 0.03, 0.09$ and 0.15) at 2 K. 100
- Table 5.1:** btained parameters from Hall effect measurements, SdH calculation and Ioffe - Regel parameter. 117
- Table 6.1.** All the obtained parameters from Hall and LL calculations. 135
- Table 6.2.** The value of First order temperature coefficient of each Raman mode for $\text{Bi}_{1.94}\text{Fe}_{0.06}\text{Se}_{2.79}\text{S}_{0.21}$ and $\text{Bi}_{1.82}\text{Fe}_{0.18}\text{Se}_{2.79}\text{S}_{0.21}$ 144

Preface

Three-dimensional (3D) topological insulators are a new state of quantum matter characterized by nontrivial bulk band topology. The nontrivial state originates from band inversion. In the Brillouin zone, there are some time-reversal invariant points at which band inversion occurs due to spin-orbit coupling. Topological insulators have insulating bulk and conducting surface states with a Dirac-cone-like dispersion. In 3D topological insulator surface states possess an odd number of massless Dirac cones. The Dirac crossing point is protected against small perturbations by time-reversal symmetry, which leads to a variety of effects. The gapless surface state of TI gives novel phenomena such as the Quantum spin Hall effect, a large value of Magneto-resistance, and another interesting quantum phenomenon such as weak antilocalization (WAL). Such exotic properties of TIs make them the future of next-generation spintronic devices.

The surface state of a topological insulator remains unaffected from nonmagnetic dopants or defects but can be modified by breaking time-reversal symmetry (TRS). On introducing magnetism in a topological insulator, Time reversal symmetry can be broken, which leads to the new path of magnetic monopoles, quantum anomalous Hall effect, and novel magnetoelectric quantum states. The possibility of topological superconductivity, Majorana fermions, and exciton condensation in TIs are fascinating. The Dirac cone-like dispersion of topological surface state (TSS) in Bi_2Te_3 , Bi_2Se_3 , and Sb_2Te_3 have been studied using Angle-resolved photoemission spectroscopy (ARPES). Quantum magnetotransport phenomena such as WAL, Shubnikov-de Hass (SdH) oscillations, Aharonov-Bhomb oscillations are associated with the surface states. However, it is very difficult to differentiate between the bulk and surface state. Besides the TSS, the bulk states in Bi_2Se_3 are of great

Preface

interest as their spin splitting is found to be twice the cyclotron energy observed in quantum oscillation.

The present thesis is focused on the magnetotransport, ARPES, the thermoelectric study of pure and doped Bi_2Se_3 , Bi_2Te_3 and Sb_2Te_3 TIs. This thesis contains the study of $\text{Bi}_{2-x}\text{M}_x(\text{SeS})_3$ indicates that surface magnetic ordering may or may not break the time-reversal symmetry (TRS). In contrast, bulk magnetic ordering breaks the TRS suggesting the potentiality of these materials for spintronic application. The angle resolved photo-emission spectroscopy (ARPES) study and magneto-transport properties of $\text{Bi}_2\text{Cu}_x\text{Te}_{3-x}$ have been investigated. In $\text{Bi}_{1.5}\text{Sb}_{0.5}\text{Te}_{1.3}\text{Se}_{1.7}$ system, Both the positive magnetoresistance (p-MR) and negative magnetoresistance (n-MR) under perpendicular magnetic field as well as a change-over from Weak Anti Localization (WAL) to Weak Localization (WL) are observed. For a systematic discussion, this thesis has been organized into six chapters.

In **Chapter 1**, physical properties of TIs, like TRS, spin momentum locking, absence of backscattering, topological Hall effect and historical developments of TIs and WSMs are discussed. The chapter also deals with other issues like the concept of Berry phase, Shubnikov-de Haas (SdH) Oscillations, WAL effect, the role of broken symmetry etc. A brief bibliographic survey is covered in the chapter.

In **Chapter 2**, the synthesis processes that have been used to grow TIs and WSMs single crystal samples and different experimental tools which have been adapted for the characterization of single-crystal samples are addressed in detail. The cryogenic techniques incorporated for transport and magnetic properties measurement, such as physical property measurement system (PPMS) and magnetic properties measurement system (MPMS) are

Preface

discussed. The basic principle of photoemission spectroscopy, such as angle-resolved photoemission spectroscopy (ARPES) is also considered in this chapter.

In **chapter 3**, The Hall effect, angle-resolved photoemission spectroscopy (ARPES) and magnetization of $\text{Bi}_{2-x}\text{M}_x(\text{SeS})_3$ (with $\text{M}=\text{Fe}, \text{Mn}$) have been investigated. In Fe doped $\text{Bi}_2(\text{SeS})_3$, the presence of both the electron-mediated RKKY coupling and carrier-independent van Vleck magnetism have been demonstrated. On the other hand, in Mn-doped sample, hole-mediated RKKY coupling is observed. The result from the DFT calculation also supports this experimental interpretation. Furthermore, both ARPES and magnetic studies indicate that surface magnetic ordering may or may not break the time-reversal symmetry (TRS), whereas bulk magnetic ordering breaks the TRS. This observation suggests the usefulness of TI-based devices for spintronics.

In **Chapter 4**, the ARPES and magneto-transport properties of $\text{Bi}_2\text{Cu}_x\text{Te}_{3-x}$ single crystals have been investigated. ARPES study indicates the clear existence of surface states in the as-prepared samples. The band gap for $x=0.03$ is ~ 5 meV, and that for the $x=0.15$ sample, the value is ~ 16 meV. The presence of Cu introduces magnetic ordering in Bi_2Te_3 which is clear from magnetic measurement. The occurrence of anomalous Hall effect is not due to the magnetic ordering but due to the 2D transport as is clear from SdH oscillation and from ARPES result.

In **Chapter 5**, the Single-phase and single-crystalline nature of the samples were established from XRD and Laue's diffraction patterns. The insulating character has been confirmed from resistivity analysis which is a consequence of the reduction in anti-site defects with sulphur doping. Furthermore, both p-MR and n-MR have been found on account of crossover from WAL to WL. From the ARPES measurement, it has been observed that on

Preface

increasing the doping concentration of sulphur, the gap is closed at the DP and DP lifts upwards. Overall, the role of sulphur doping is becoming very interesting.

In **Chapter 6**, the electron-phonon interaction plays a vital role in the transport properties of Fe and S doped Bi_2Se_3 . After doping magnetic elements, the surface state still exists and provides unsaturated linear Magneto-resistance from which we calculated SdH oscillation. Resistivity, Thermoelectric study and Raman study of these samples supports the role of electron-phonon interaction in the transport properties.

Chapter 7, this chapter contains the summary of the present thesis with a brief glimpse of future studies.